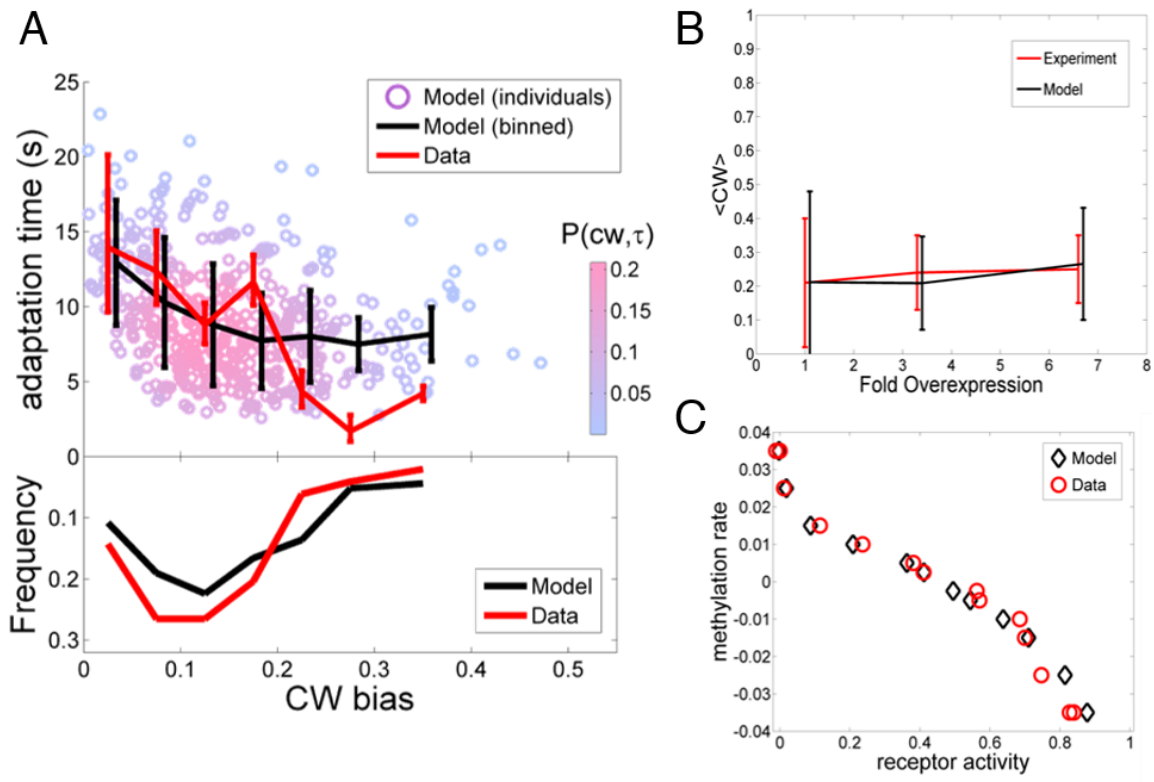

Figure 2 – figure supplement 1 | Comparing the model to single cell and population averaged measurements. The same set of model parameter values is used for all the plots. **A**. Adaptation time and motor clockwise (CW) bias. Bottom: normalized histogram of motor clockwise bias in the population. Top: The mean and standard deviation of adaptation time in each bin of CW bias. Red lines: experimental data from Park et al.[1]. Black lines: model. Circles: Individual cells from the model. Color: probability density. **B**. Population-averaged CW bias as a function of fold changes in mean expression level of all pathway proteins after Kollmann et al.[2]. Red: data from Kollmann et al. Black: model. **C**. Population-averaged methylation rate as a function of population-averaged receptor activity obtained by exposing cells to exponential ramps of methyl-aspartate as described in Shimizu et al.[3]. Red circles: data from Shimizu et al. Black: simulation of model.

References

1. Park H, Pontius W, Guet CC, Marko JF, Emonet T, et al. (2010) Interdependence of behavioural variability and response to small stimuli in bacteria. Nature 468: 819-823.
2. Kollmann M, Lovdok L, Bartholome K, Timmer J, Sourjik V (2005) Design principles of a bacterial signalling network. Nature 438: 504-507.
3. Shimizu TS, Tu Y, Berg HC (2010) A modular gradient-sensing network for chemotaxis in Escherichia coli revealed by responses to time-varying stimuli. Mol Syst Biol 6: 382.

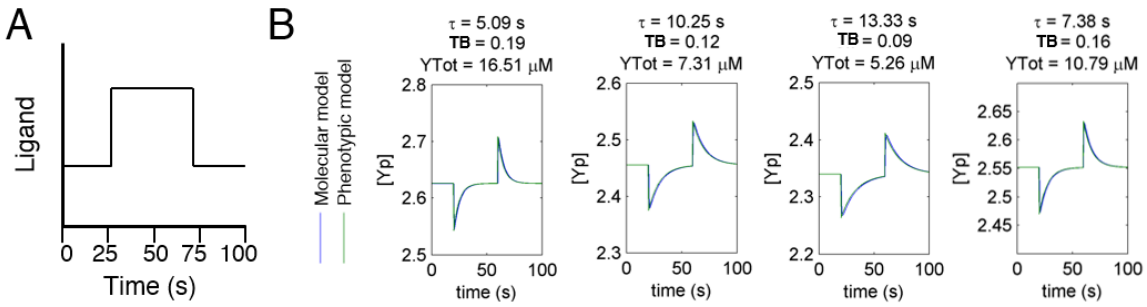

Figure 2 – figure supplement 2 | Agreement between protein model and parametric dynamics model. **A**. Cartoon of step function of ligand delivered to immobilized cells in simulation to test response dynamics. **B**. Direct comparison of response of molecular model (blue) and phenotypic model (green) with the same parameters to stimulus of the form in A illustrating close agreement.

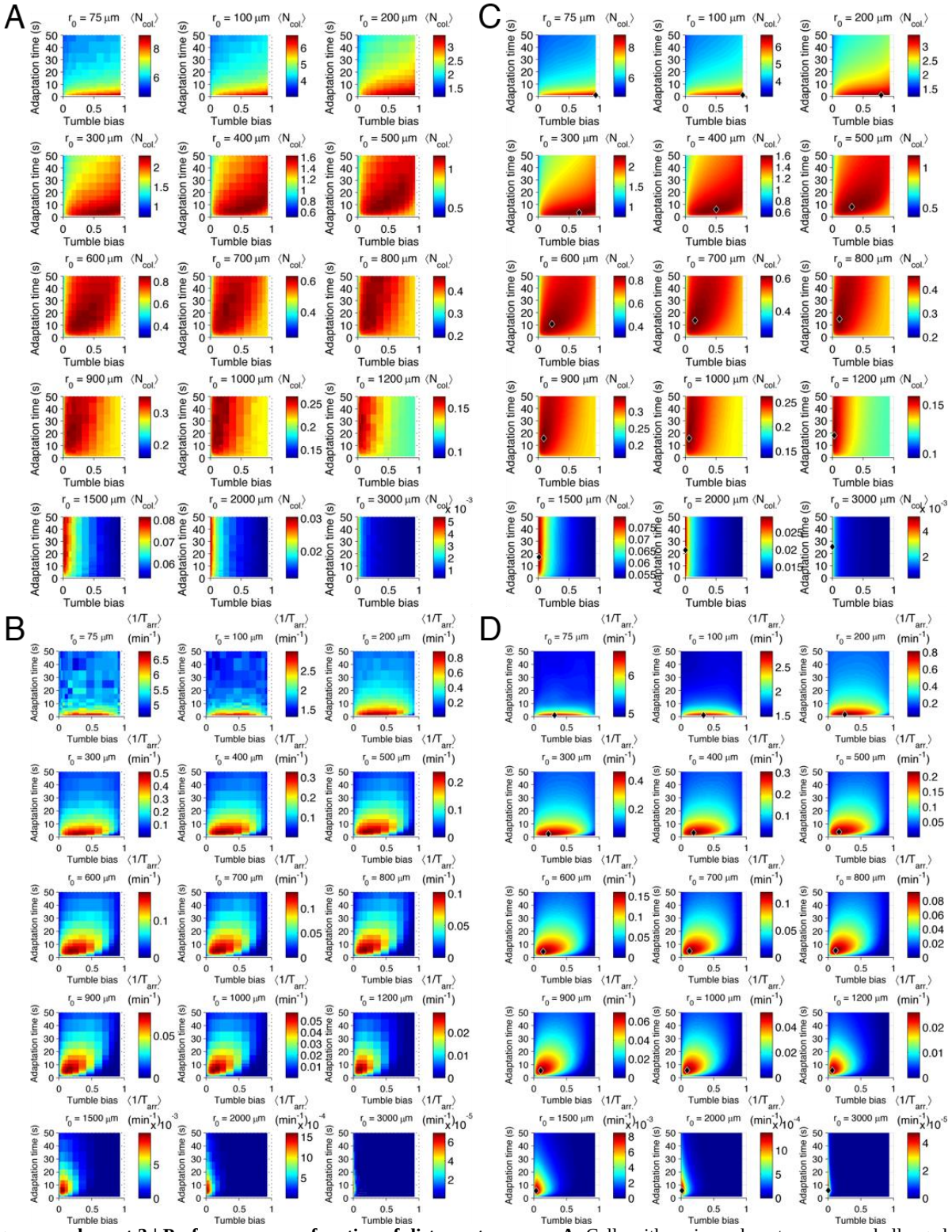

Figure 2 – figure supplement 3 | Performance as a function of distance to source. A. Cells with various phenotypes were challenged to forage a source presented at varying distances, r_0 from 75μm to 3mm. Between 6000 and 30000 replicates were simulated for each phenotype. $\langle N_{col.} \rangle$: the average nutrient collected by all replicates of a given phenotype in μmol. **B**. Same as A but for a colonization challenge; $\langle 1/T_{arr.} \rangle$: the average reciprocal-of-arrival-time of all of the replicates of a given phenotype in min^{-1}. **C**. Data in A smoothed with a Gaussian filter and resampled on a higher resolution grid of phenotypic parameters. Diamond: phenotype with highest performance. **D**. Same as C but with the data in B

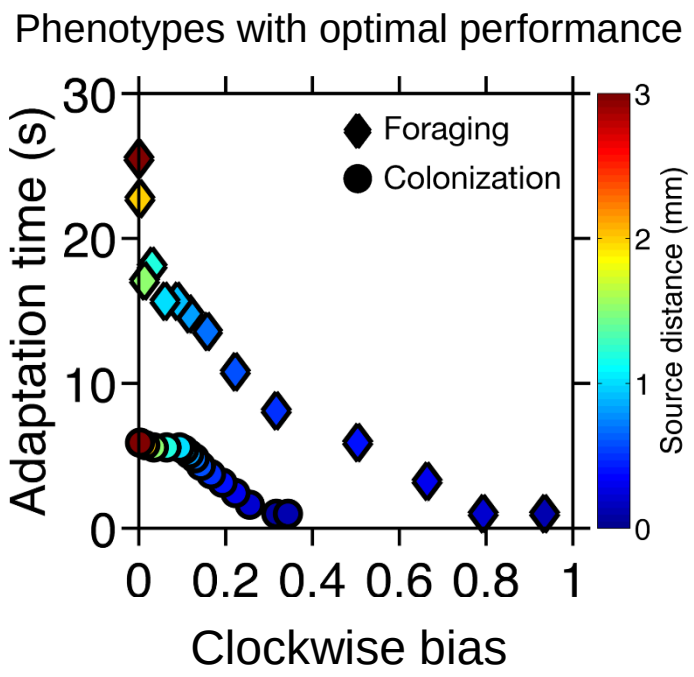

Figure 2 – figure supplement 4 | Optimal phenotypes as a function of source distance. For each source distance and each task, the phenotype with highest performance was identified as shown in Figure 2 – figure supplement 3. The clockwise bias and adaptation time of these phenotypes are shown with the marker color corresponding to the distance to the source. Diamonds: foraging case. Circles: colonization case.

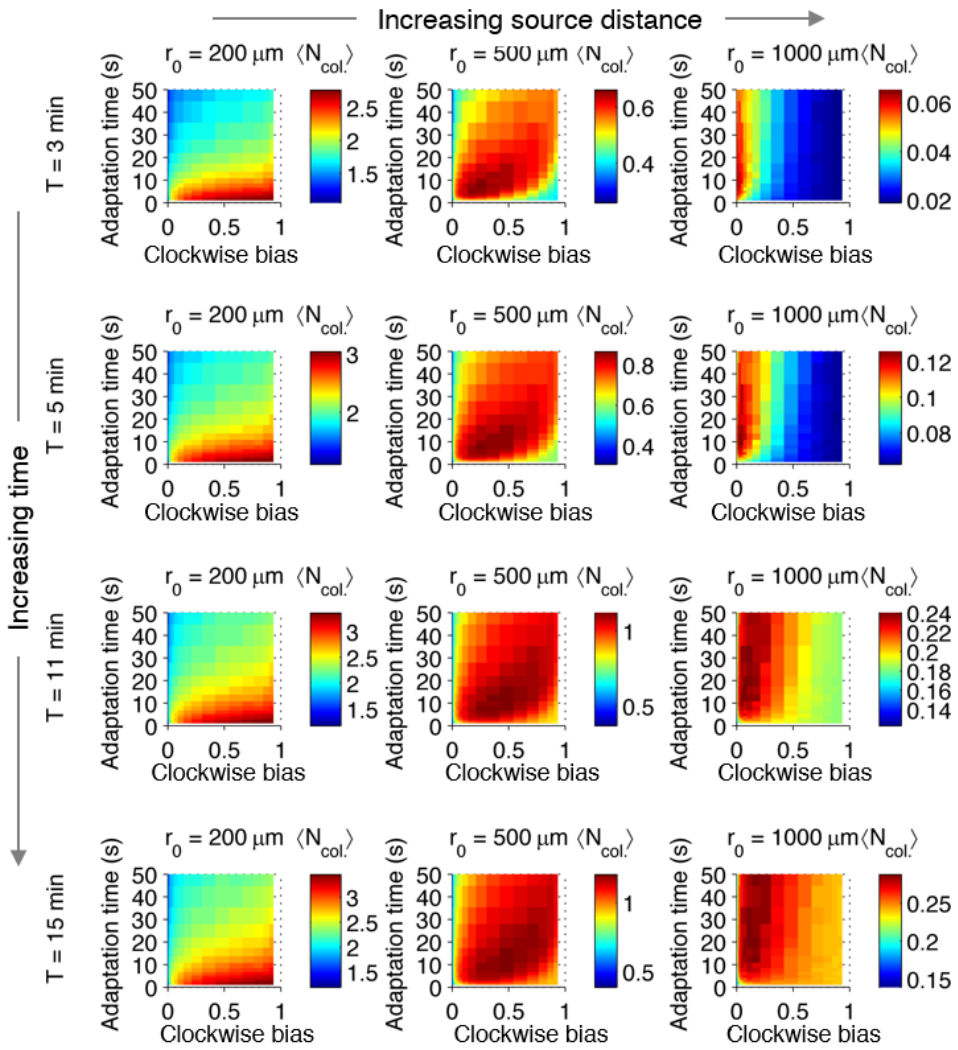

Figure 2 – figure supplement 5 | Effect of time restrictions on foraging performance. Cells were challenged to forage sources that appeared at distances of 200, 5000, or 1000 µm away (columns from left to right). Different amounts of time were allotted to cells to accumulate ligand: 3 min, 5 min, 11 min, 15 min (rows from top to bottom). $\langle N_{col.} \rangle$: the average nutrient collected by replicates of a given phenotype in µmol.

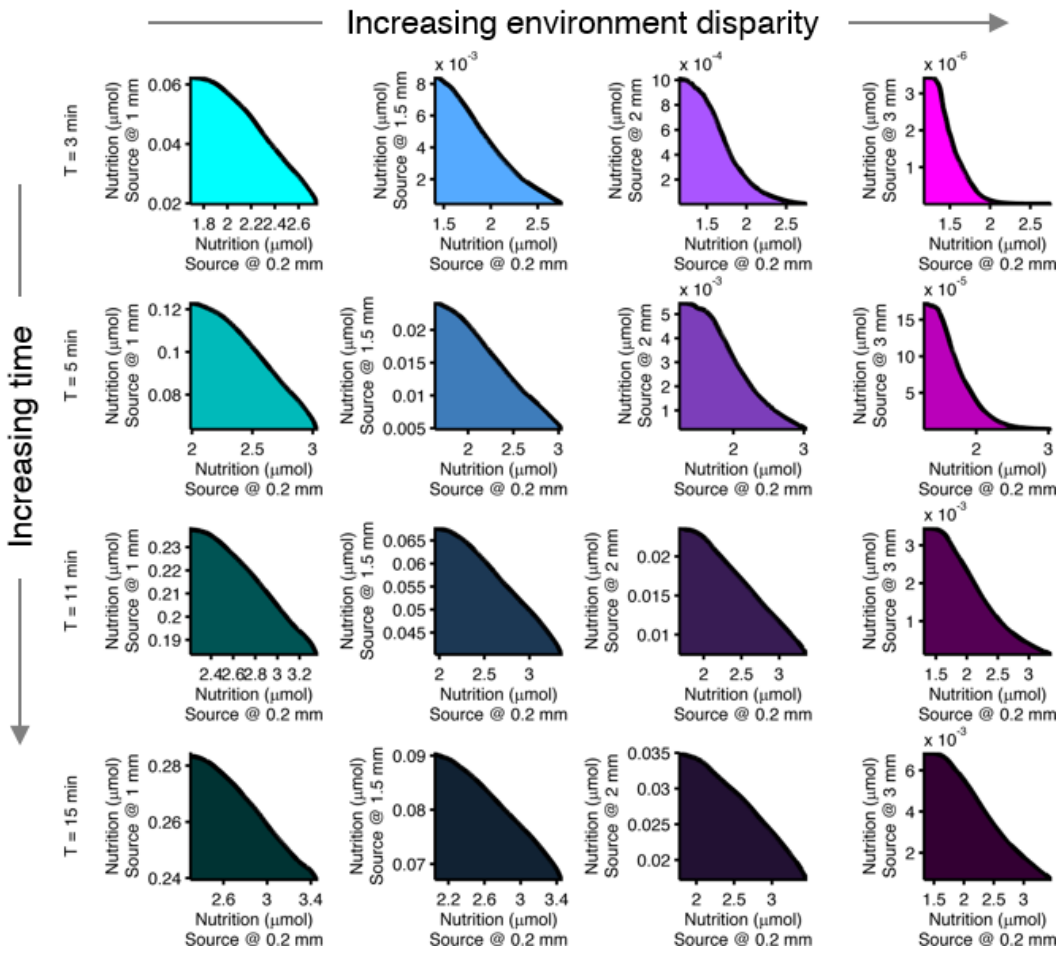

Figure 2 – figure supplement 6 | Effect of time limits on near/far foraging trade-offs. Trade-offs in performance between foraging near and far sources are shown. From left to right (cyan to magenta), the far case is progressively more distant compared to the near case: 1mm, 1.5mm, 2mm, 3mm. From top to bottom (bright to dark colors), the time allotted is increasing: 3 min, 5min, 11min, 15min. Reduced time allotment makes the front (black line) more concave for the same pair of environments.

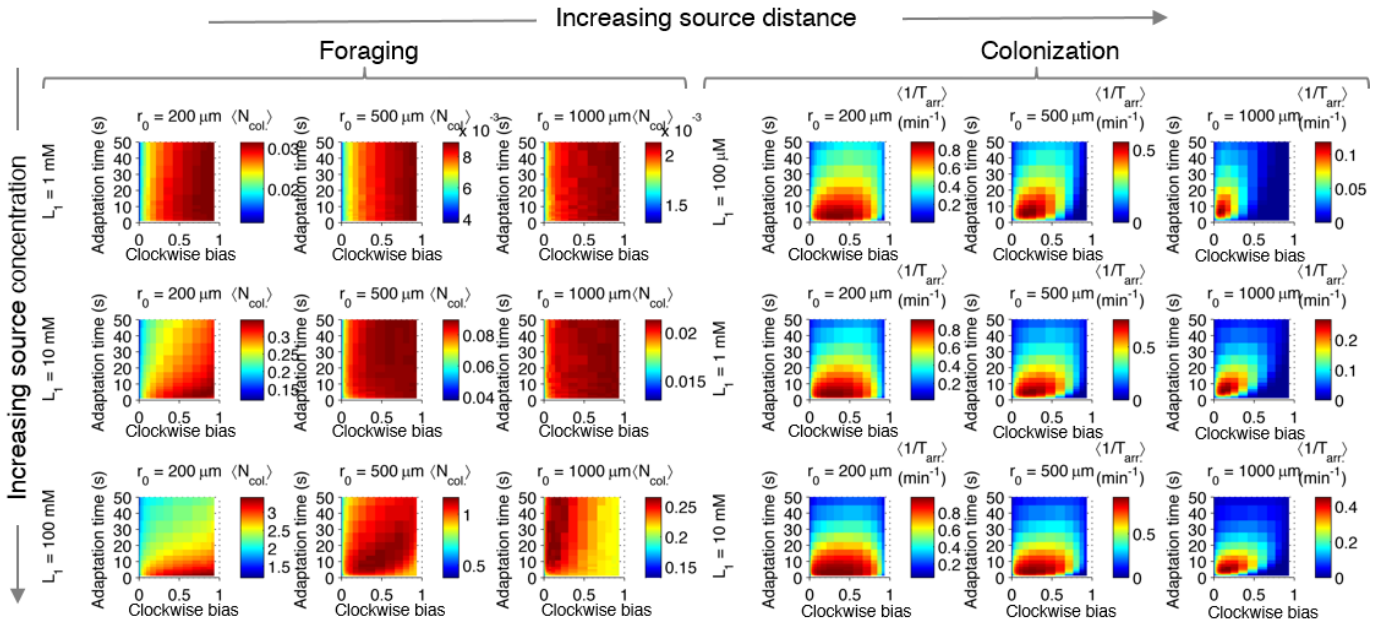

Figure 2 – figure supplement 7 | Effect of source concentration on performance. Performance calculate and plotted as described in Figure 2 – figure supplement 3, but for different concentrations at the source. Left block ("Foraging"): foraging performance for increasing source distance (columns) and increasing source concentration (rows): L_1 = 1 mM, 10 mM, 100 mM. Right block ("Colonization") colonization performance for increasing source distance (columns) and increasing source concentration (rows): L_1 = 100 μM, 1 mM, 10 mM.

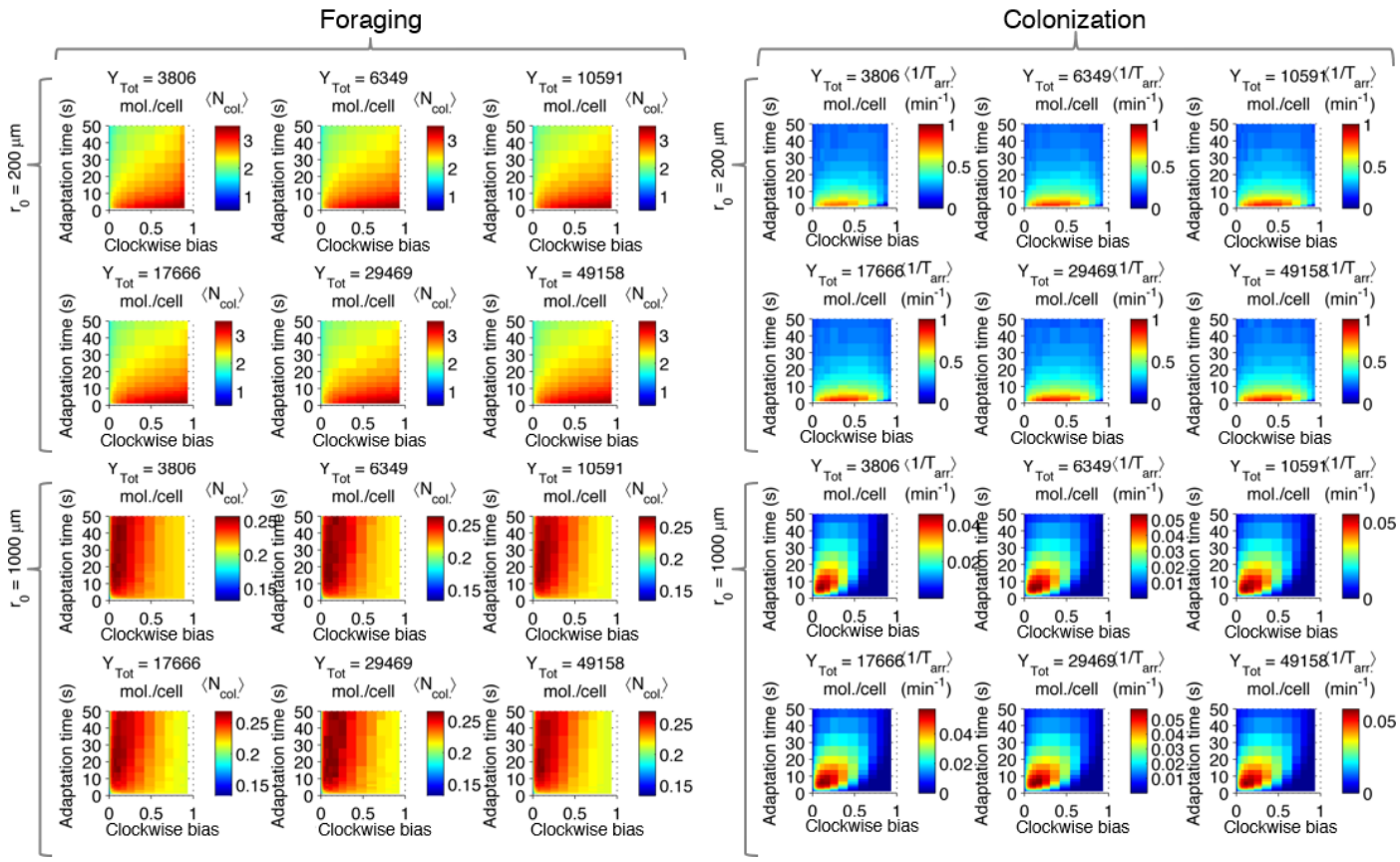

Figure 2 – figure supplement 8 | Effect of CheY-P dynamic range on performance. Left block ("Foraging"): foraging performance for near (200 µm) and far (1000 µm) sources and increasing CheY-P dynamic range, which was changed through the total number of CheY molecules, Y_{tot}, as described in the SI. Right block ("Colonization") same as left block but for colonization.

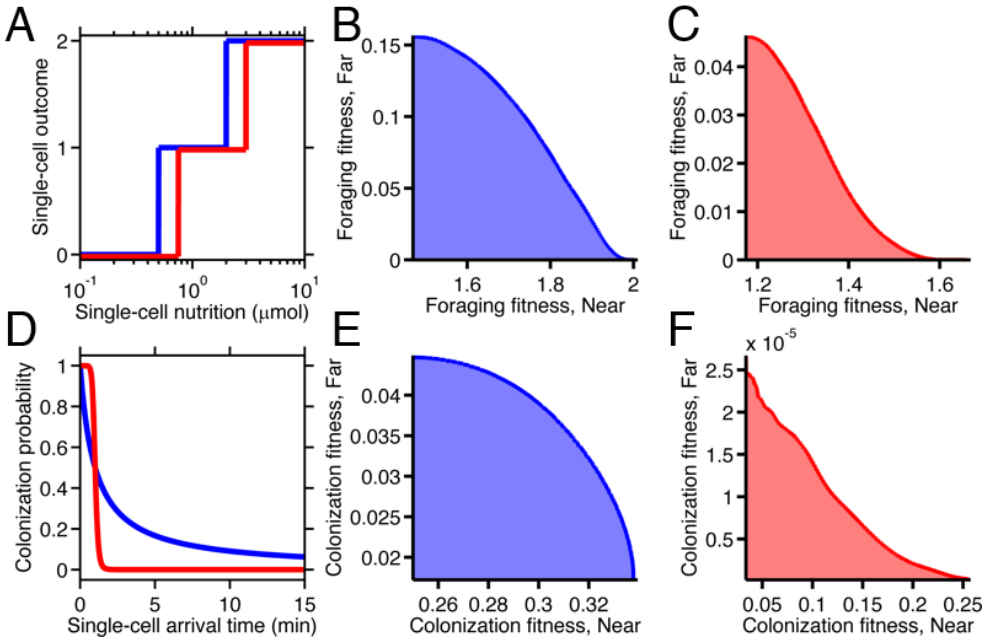

Figure 4 – figure supplement 1 | Fitness trade-offs under alternate models of selection. A. Model of discrete physiological transitions applied to the chemotactic foraging challenge. Each individual replicate is given a number of progeny (0, 1, or 2) based on a two-step function of the nutrition they achieve from chemotaxis. For each phenotype, the foraging fitness is the average progeny across replicates. The effect of more (red) and less (blue) stringent nutrient requirements are compared. Survival requirement: 0.5 µmol (blue), 0.75 µmol (red), Division requirement: 2 µmol (blue), 3 µmol (red). **B–C**. Beginning with the foraging performance trade-off in Figure 4B, application of the survival model in A gives rise to either a weak (B) or strong (C) fitness trade-off, depending on where the thresholds and steepness are low (blue curve in A) or high (red curve in A). **D**. Probabilistic model of survival applied to the chemotactic colonization challenge. Each individual replicate survives has chance to survive depending on how soon it arrives. For each phenotype, the colonization fitness is the probability to colonize measured over all replicates. The effect of more (red) and less (blue) stringent survival functions are compared. Time threshold in both cases is 1 min with dependency 1 (blue) or 10 (red). **E–F**. Beginning with the arrival performance trade-off in Figure 4E, application of the selection model in C gives rise to either a weak (E) or strong (F) fitness trade-off.

Table S1.

Receptor Parameters				
Name	Description	Type	Value	Reference
ε_0	Basal energy of receptor cluster	Fixed	6 k_BT	Shimizu et al. 2010[1]
ε_1	Receptor energy change per methyl group addition	Fixed	-1 k_BT	Shimizu et al. 2010[1]
K_{TAR}^{off}	Tar_{off}–meAsp diss. constant	Fixed	18.2 μM	Shimizu et al. 2010[1]
K_{TAR}^{on}	Tar_{on}–meAsp diss. constant	Fixed	3000 μM	Shimizu et al. 2010[1]
K_{TSR}^{off}	Tsr_{off}–meAsp diss. constant	Fixed	10^4 μM	Endres and Wingreen, 2006[2]
K_{TSR}^{on}	Tsr_{on}–meAsp diss. constant	Fixed	10^9 μM	Endres and Wingreen, 2006[2]
N_{TAR}	Number of Tar receptor dimers	Fixed	2 (6*)	Shimizu et al. 2010[1], Li and Hazelbauer, 2004[3]
N_{TSR}	Number of Tsr receptor dimers	Fixed	4 (0*)	Shimizu, et al. 2010[1], Li and Hazelbauer, 2004[3]
Signaling Parameters				
Name	Description	Type	Value	Reference
k_r	Catalytic rate of CheR	Fitted	350 s^{-1}	*this study*
K_r	Equilibrium constant of CheR activity	Fitted	300 μM	*this study*
k_b	Catalytic rate of CheB	Fitted	266 s^{-1}	*this study*
K_b	Equilibrium constant of CheB activity	Fitted	200 μM	*this study*
a_P	CheA autophosphorylation rate	Fitted	12.5 s^{-1}	*this study*
a_B	Rate of CheB phosphorylation by CheA	Fixed	15 μM^{-1} s^{-1}	Stewart, Jahreis, and Parkinson, 2000[4]
d_B	CheB autodephosphorylation rate	Fixed	0.5 s^{-1}	Stewart, 1993[5], Kentner and Sourjik, 2006[6]
a_Y	Rate of CheY phosphorylation by CheA	Fixed	50 μM^{-1} s^{-1}	*this study*
d_Z	Rate of CheY desphosphorylation by CheZ	Fixed	5 μM^{-1} s^{-1}	*this study*
Motor Parameters				
Name	Description	Type	Value	Reference
ω_0	Basal switching frequency	Fixed	1.3 s^{-1}	Sneddon et al., 2012[7], Cluzel et al., 2000[8]
g_1	Transition energy of motor	Fixed	40 k_BT	Sneddon et al., 2012[7], Cluzel et al., 2000[8]
K_D	Dissociation constant of CheY-motor interaction	Fixed	3.06 μM	Sneddon et al., 2012[7], Cluzel et al., 2000[8]
Simulation Parameters				
Name	Description	Type	Value	Reference
v	Cell speed	Fixed	20 μm s^{-1}	Sneddon et al., 2012[7], Berg and Brown, 1972[9]
D_{ROT}	Rotational diffusion	Fixed	0.062 rad s^{-1}	Sneddon et al., 2012[7], Berg and Brown, 1972[9]
k_{rot}	Post-tumble redirection angle Gamma distribution shape parameter	Fixed	4	Sneddon et al., 2012[7], Berg and Brown, 1972[9]
θ_{rot}	Post-tumble redirection angle Gamma distribution scale parameter	Fixed	18.32	Sneddon et al., 2012[7], Berg and Brown, 1972[9]
D	Diffusion coefficient of methyl-aspartate	Fixed	550 μm^2 s^{-1}	Lewus et al., 2001[10]

k	Nutrient pickup rate	Fixed	10^{-4} μmol/μM/s	*This study*
Gene expression parameters				
Name	Description	Type	Value	Reference
$<T>$	Population mean receptors per cell (Tar + Tsr)	Population variable, fixed during fitting	15000 mol./cell	Li and Hazelbauer, 2004[3]
$<A>$	Population mean CheA proteins per cell	Population variable, fixed during fitting	6700 mol./cell	Li and Hazelbauer, 2004[3]
$<W>$	Population mean CheW proteins per cell	Population variable, fixed during fitting	6700 mol./cell	Li and Hazelbauer, 2004[3]
$<R>$	Population mean CheR proteins per cell	Population variable, fixed during fitting	140 mol./cell	Li and Hazelbauer, 2004[3]
$<B>$	Population mean CheB proteins per cell	Population variable, fixed during fitting	240 mol./cell	Li and Hazelbauer, 2004[3]
$<Y>$	Population mean CheY proteins per cell	Population variable, fixed during fitting	8200 mol./cell	Li and Hazelbauer, 2004[3]
$<Z>$	Population mean CheZ proteins per cell	Population variable, fixed during fitting	3200 mol./cell	Li and Hazelbauer, 2004[3]
x	Conversion between mol./cell and μM for proteins	Fixed	833 μM/mol./cell	
A_{RB}	Translational coupling coefficient between CheR and CheB	Fixed	0.485	Lovdok et al., 2009[11]
A_{BY}	Translational coupling coefficient between CheB and CheY	Fixed	0.210	Lovdok et al., 2009[11]
A_{YZ}	Translational coupling coefficient between CheY and CheZ	Fixed	0.250	Lovdok et al., 2009[11]
η	Intrinsic noise scaling coefficient	Population variable, fitted during fitting	0.125	*this study*
ω	Extrinsic noise scaling coefficient	Population variable, fitted during fitting	0.26	*this study*

Table S1. Parameter Values and Variables.
*Values in parentheses were used when directly comparison to Shimizu et al., 2010[1] to reflect the Tsr knockout mutation used in that study.

References

1. Shimizu TS, Tu Y, Berg HC (2010) A modular gradient-sensing network for chemotaxis in Escherichia coli revealed by responses to time-varying stimuli. Mol Syst Biol 6: 382.
2. Endres RG, Wingreen NS (2006) Precise adaptation in bacterial chemotaxis through "assistance neighborhoods". Proc Natl Acad Sci U S A 103: 13040-13044.
3. Li M, Hazelbauer GL (2004) Cellular stoichiometry of the components of the chemotaxis signaling complex. J Bacteriol 186: 3687-3694.
4. Stewart RC, Jahreis K, Parkinson JS (2000) Rapid phosphotransfer to CheY from a CheA protein lacking the CheY-binding domain. Biochemistry 39: 13157-13165.
5. Stewart RC (1993) Activating and inhibitory mutations in the regulatory domain of CheB, the methylesterase in bacterial chemotaxis. J Biol Chem 268: 1921-1930.
6. Kentner D, Sourjik V (2006) Spatial organization of the bacterial chemotaxis system. Curr Opin Microbiol 9: 619-624.
7. Sneddon MW, Pontius W, Emonet T (2012) Stochastic coordination of multiple actuators reduces latency and improves chemotactic response in bacteria. Proceedings of the National Academy of Sciences of the United States of America 109: 805-810.
8. Cluzel P, Surette M, Leibler S (2000) An ultrasensitive bacterial motor revealed by monitoring signaling proteins in single cells. Science 287: 1652-1655.

9. Berg HC, Brown DA (1972) Chemotaxis in Escherichia coli analysed by three-dimensional tracking. Nature 239: 500-504.
10. Lewus P, Ford RM (2001) Quantification of random motility and chemotaxis bacterial transport coefficients using individual-cell and population-scale assays. Biotechnology and Bioengineering 75: 292-304.
11. Lovdok L, Bentele K, Vladimirov N, Muller A, Pop FS, et al. (2009) Role of translational coupling in robustness of bacterial chemotaxis pathway. PLoS Biol 7: e1000171.